Neuron, Volume *73*

Supplemental Information

The Generation of Direction Selectivity in the Auditory System

Richard I. Kuo and Guangying K. Wu

Supplemental Figures

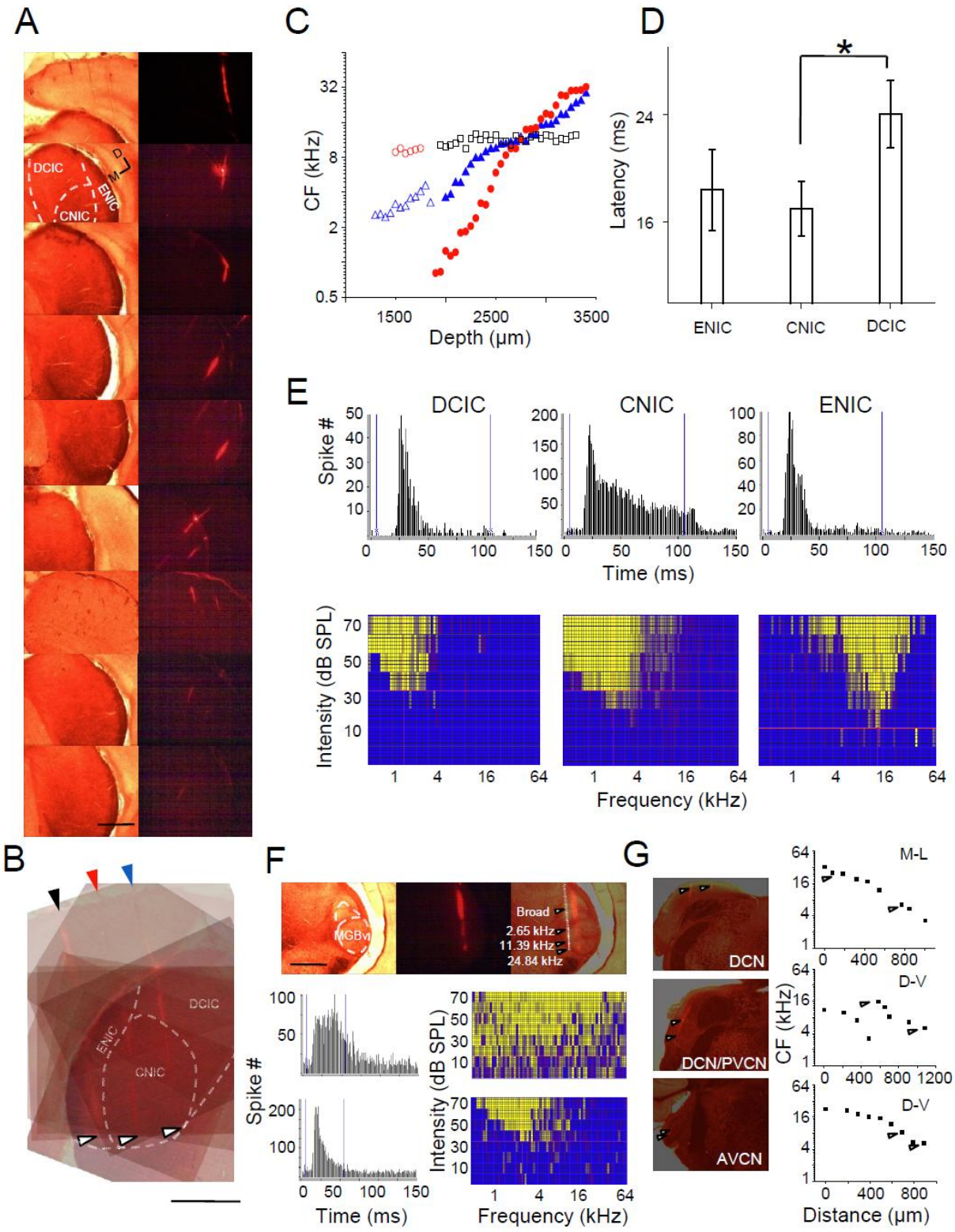

Figure S1

Figure S1. **Histology and physiological criteria for functionally identifying the subdivisions of CN, IC, and MGB**

A. Nine serial sections of the IC from the posterior to the anterior. Left, bright field images of the structure of IC; right, fluorescent images of the recording tracks labeled by DiI; D, dorsal; M, ventral; bar, 1mm.

B. Reconstruction of the whole recording tracks. Colored arrowheads, penetration sites on the surface of the brain; white arrowheads, the end points of the recording tracks; bar, 1mm.

C. CF of sampling sites along three recording tracks (blue, red, and black) illustrated in B. Filled symbol, sustained firing pattern; open symbol, transient firing pattern.

D. First-spike latencies of neurons in three subdivisions. Error bar, SD.; t-test, $p<0.005$.

E. PSTH (upper) and spike tonal receptive fields (lower) from three representative sampling sites in DCIC, CNIC, and ENIC.

F. A sample section of the MGB with a recording track identified dorsal-ventrally. Upper, bright field image, fluorescent image and overlaid image, four representative recording sites indicated by the white arrowheads and tonotopically changed CF's; lower, PSTH and spike receptive fields of representative responses of MGBd and MGBv, the two recording sites labeled with 'broad' and '2.64 kHz' in the upper panel; bar: 1mm.

G. Three sections of the CN (from posterior to anterior) with overlaid recording tracks (left) and corresponding tonotopic organizations (right). Upper, a section of DCN; M-L, tonotopic CF gradient from medial to lateral; middle, a section of DCN and PVCN; D-V, tonotopic CF gradient from dorsal to ventral with an abrupt change at the border of DCN and PVCN; lower, a section of AVCN, D-V, tonotopic CF gradient from dorsal to ventral. Whiteheads indicates recording sites; '0' coordinates indicates the first responsive recording site encountered in pre-mapping.

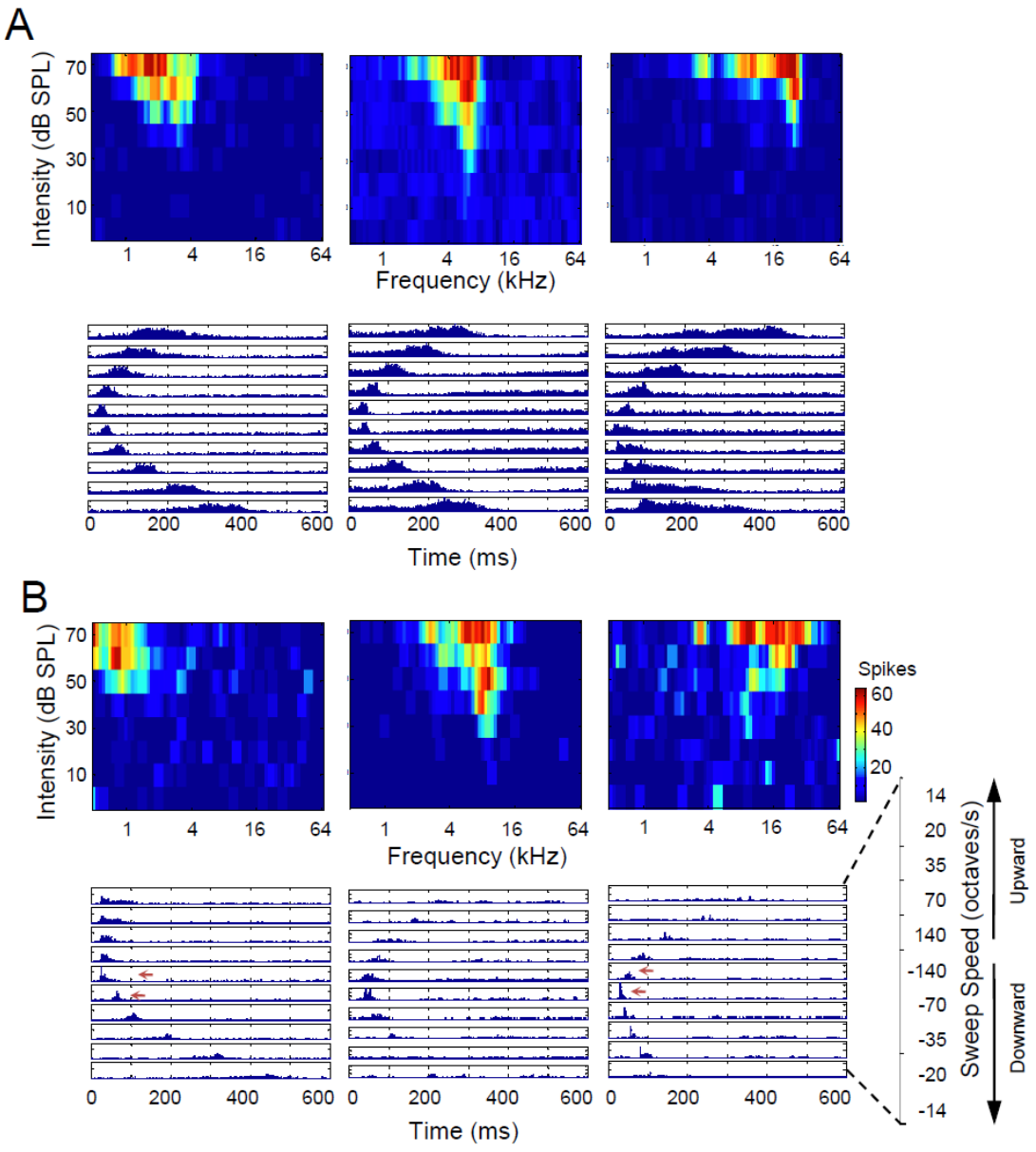
A
Intensity (dB SPL)
70
50
30
10
1
4
16
64
Frequency (kHz)
0
200
400
600
Time (ms)
B
Intensity (dB SPL)
Frequency (kHz)
Time (ms)
Spikes
60
40
20
Sweep Speed (octaves/s)
14
20
35
70
140
-140
-70
-35
-20
-14
Upward
Downward

Figure S2

Figure S2. Multi-unit recordings from the cochlear nuclei (CN) and the ventral part of medial geniculate body (MGBv)

A. Spike tonal receptive fields from three representative sampling sites in the CN (upper panels), with CF's of 2.98 kHz, 7 kHz and 21.98 kHz. PSTH of spike responses evoked by various speeds of FM sweeps in either upward or downward direction (lower panels).

B. Spike tonal receptive fields and PSTH of three sampling sites in the MGBv presented as in A, with CF's of 0.98 kHz, 8.7 kHz, and 18.6 kHz. Arrows indicate the responses evoked by a pair of FM sweeps with the same speed but in opposing directions that generate largest DSI. The range of vertical axis of each box is 0 to 20 (spike number).

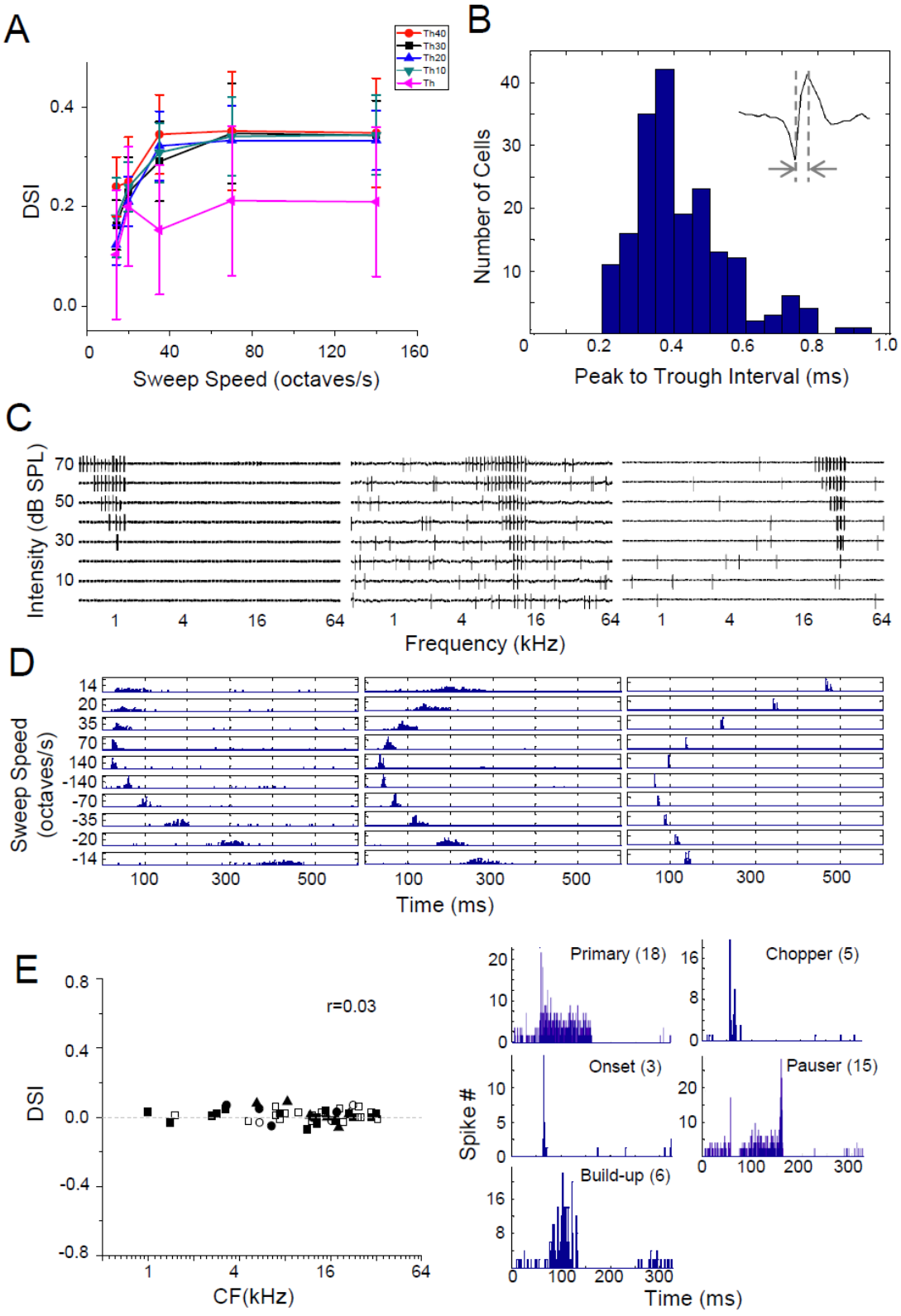
A
Th40
Th30
Th20
Th10
Th
DSI
Sweep Speed (octaves/s)
B
Number of Cells
Peak to Trough Interval (ms)
C
Intensity (dB SPL)
Frequency (kHz)
D
Sweep Speed (octaves/s)
Time (ms)
E
r=0.03
DSI
CF(kHz)
Primary (18)
Chopper (5)
Onset (3)
Pauser (15)
Build-up (6)
Spike #
Time (ms)

Figure S3

Figure S3. Analysis of spike responses of IC and CN neurons to FM sweeps

A. DSI v.s. FM sweep speed at various sound intensities. Averaged absolute DSI's from multi-unit recordings of five sampling sites in the IC. Pink, at the intensity threshold; Green, 10 dB above the threshold; Blue, 20 dB above the threshold; Black, 30 dB above the threshold; Red, 40 dB above the threshold; bar, SD.

B. Distribution of IC neurons according to their spike waveforms. Data from cell-attached recordings were used (n=189). Inset represents an example spike waveform for measuring peak to trough interval.

C. Spike tonal receptive fields consist of raw traces of three representative CN neurons acquired by cell-attached recording with low, middle and high CF's. For each combination of frequency and intensity, single cell responses within a 100ms of time window after the start of sound stimulation were shown.

D. PSTH's of spike responses of neurons in (C) evoked by various speeds of FM sweeps, the stimulation starts at 10 ms. The range of vertical axis of each box is 0 to 15 (spike number).

E. DSI-CF dependence of single neurons in the CN (n=47). Filled square, pauser; open square, primary; filled circle, chopper; open circle, onset; triangle, build-up; correlation coefficient r is shown.

F. Five representative response types of CN neurons recorded. 100 ms CF tones were delivered at 50 ms. The number for each type indicated in parentheses.

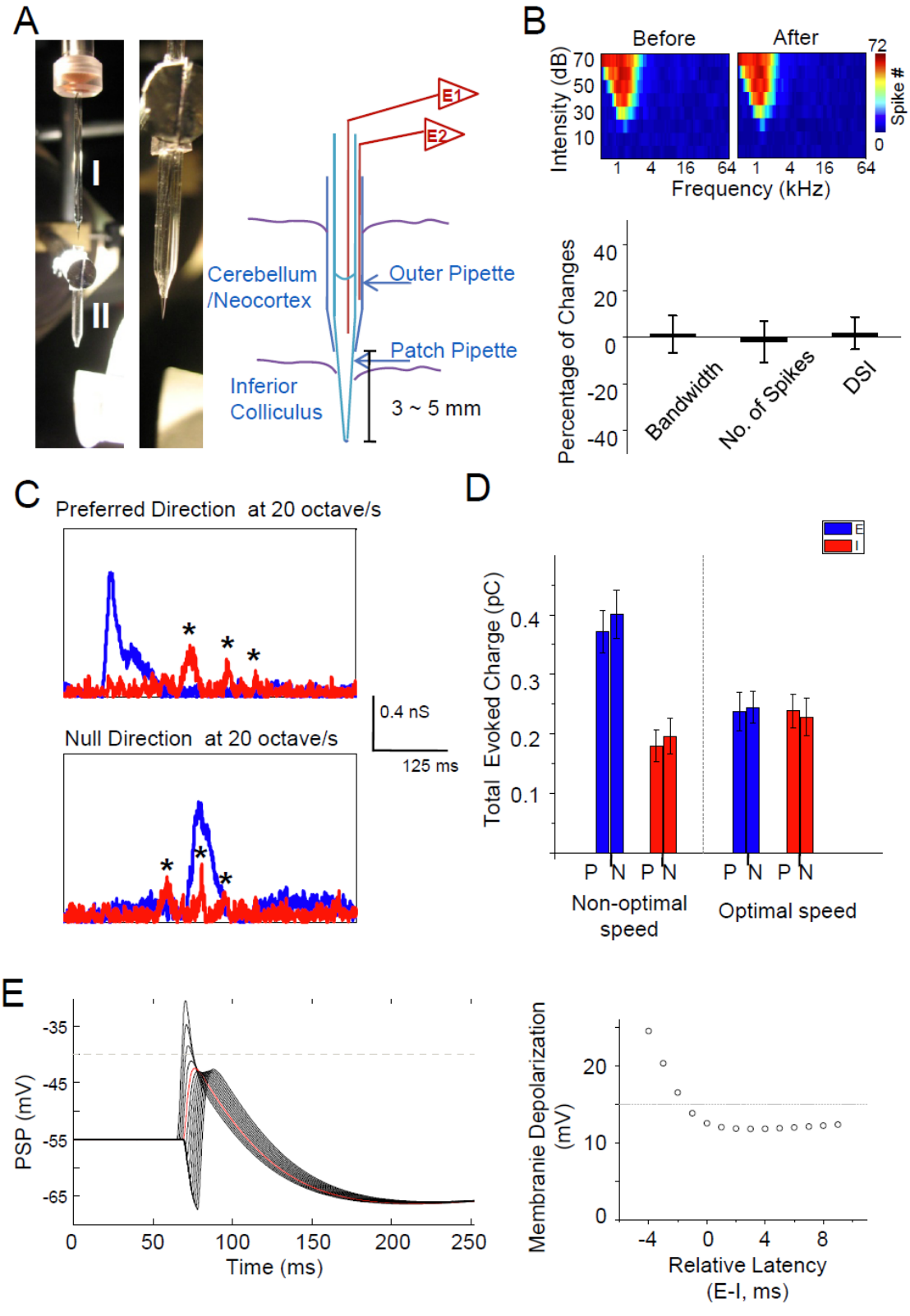
A
I
II
E1
E2
Cerebellum
/Neocortex
Outer Pipette
Patch Pipette
Inferior
Colliculus
3 ~ 5 mm
B
Before
After
Intensity (dB)
70
50
30
10
1
4
16
64
Frequency (kHz)
72
Spike #
0
Percentage of Changes
40
20
0
-20
-40
Bandwidth
No. of Spikes
DSI
C
Preferred Direction at 20 octave/s
Null Direction at 20 octave/s
0.4 nS
125 ms
D
E
I
Total Evoked Charge (pC)
0.4
0.3
0.2
0.1
P N P N
P N P N
Non-optimal
speed
Optimal speed
E
PSP (mV)
-35
-45
-55
-65
0
50
100
150
200
250
Time (ms)
Membranie Depolarization
(mV)
20
10
0
-4
0
4
8
Relative Latency
(E-I, ms)

Figure S4

Figure S4. Measurement of synaptic inputs of IC neurons

A. Right, coaxial electrodes driven by two separated micro-manipulators (I and II), before and after the inner patch electrode passes through the outer electrode; left, a schematic configuration of coaxial electrode system. The outer electrode (E2) was positioned about 100-200 μm above the target region (e.g. inferior colliculus in our experiment). The inner electrode (E1) was then advanced to blindly search for neurons and used to perform intracellular recordings.

B. Upper, spike tonal receptive fields of a recording site before (left) and after (right) the removal of a small portion of parietal-occipital cortex for IC recordings; lower, percentage change of responding frequency bandwidth, spike number and DSI before and after the neocortex removal. Error bar, SD.

C. Synaptic inputs in response to opposing directions at non-optimal speed. FM sweep-evoked excitatory (blue) and inhibitory synaptic conductance (red) of the neuron presented in Figure 4A (lower panel). Asterisks indicate the scattered major inhibitory inputs.

D. Calculated magnitudes (total evoked electric charge) of excitatory (blue) and inhibitory (red) inputs in (C). P, preferred direction; N, null direction; bar, SEM.

E. Modeling the impacts of temporal asymmetry of excitatory and inhibitory inputs on membrane potential responses (see supplemental information). Left, simulated membrane potential responses by integrating the excitatory and inhibitory inputs with varying temporal relationships, red trace indicates membrane potential changes evoked by excitatory and inhibitory inputs with the same onset latency; right, peak depolarization v.s. relative latency between excitation and inhibition; dashed gray line indicates the spike threshold.

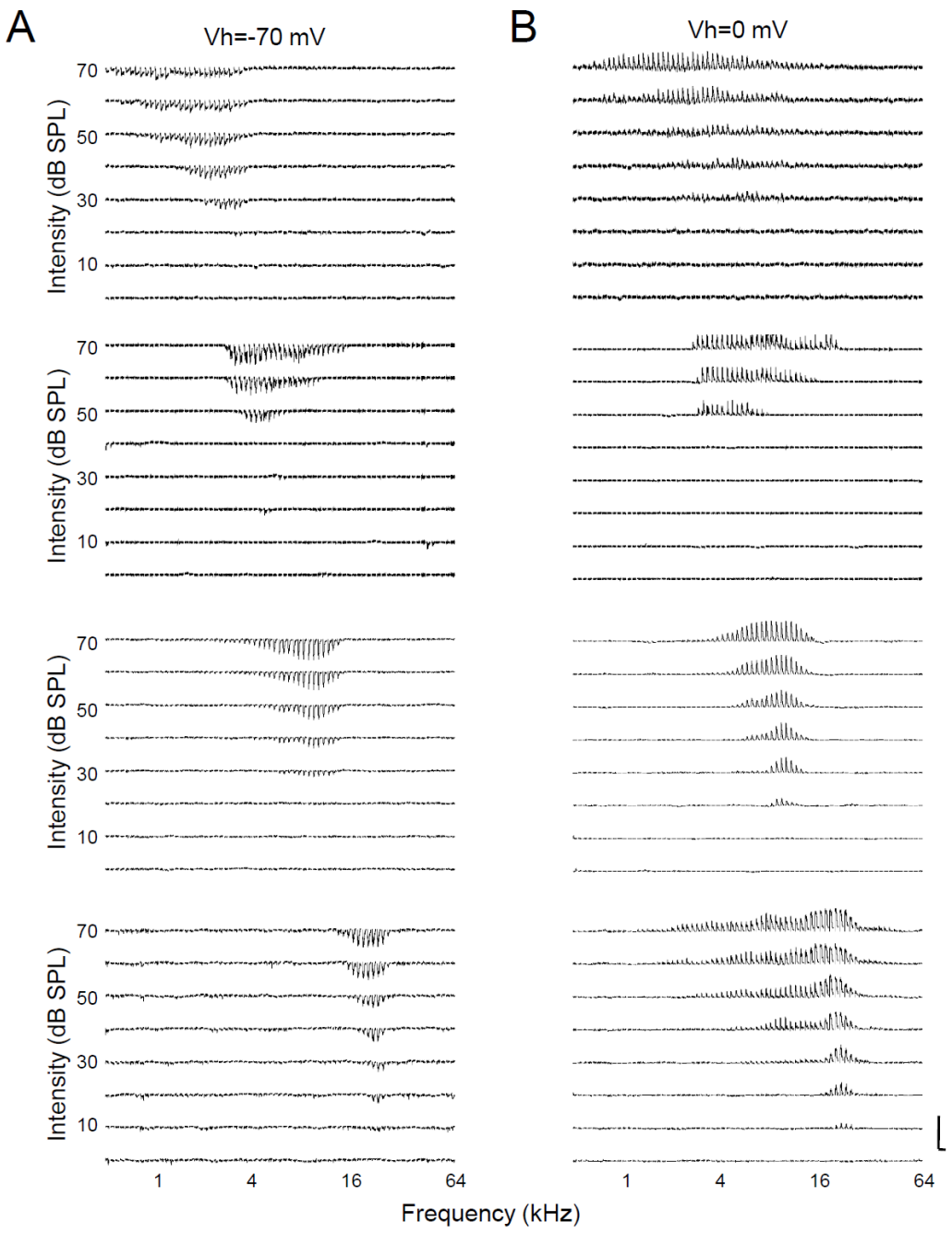
A
Vh=-70 mV
B
Vh=0 mV
Intensity (dB SPL)
70
50
30
10
1
4
16
64
Frequency (kHz)

Figure S5

Figure S5. Raw traces of excitatory and inhibitory synaptic tonal receptive fields of neurons presented in Figure 5

A and B, excitatory (A) and inhibitory (B) synaptic currents recorded in example neurons at -70 mV and 0mV, respectively, in response to pure tones of various frequencies and intensities. Each small trace represents response to a tone (averaged from two to four repeats). Vertical bar indicates the scale of 500 pA of the current amplitude; horizontal bar indicates the scale of 50 ms of time.

Supplemental Experimental Procedures

Modeling of the contribution of synaptic input timing to the membrane potential changes

To further examine the contribution of the timing between excitation and inhibition to the direction selectivity, a single-compartment neuron model was used to simulate membrane potential responses, which are resulted from the synaptic inputs with parameters derived from our experiments with various temporal relationships drawn from Figure 4E. The results were shown in Figure S4E.

The excitatory and inhibitory synaptic inputs to such a neuron model were simulated by the following equation (Zhang et al., 2003; Zhou et al., 2010):

$$I(t) = a * H(t - t_0) * (1 - e^{-(t-t_0)/\tau_{rise})}) * e^{-(t-t_0)/\tau_{decay})}$$

I(t): synaptic input current;
a: factor to determine the amplitude to synaptic currents;
H(t): Heaviside step function;
t_0: onset delay of the input;
τ_{rise}: time constant for the rising phase;
τ_{decay} : time constant for the decay phase;

The parameters were chosen for fitting the averaged shape of the recorded synaptic responses.

Membrane potential changes were simulated from the modeled synaptic inputs. An integrate-and-fire model was used as previously described (Wehr and Zador, 2003; Liu et al., 2007; Zhou et al., 2010; Somers et al., 1995):

$$Vm(t + dt) = -\frac{dt}{C}\left[Ge(t) * (Vm(t) - Ee) + Gi(t) * (Vm(t) - Ei) + Gr(Vm(t) - Er)\right] + Vm(t)$$

Vm(t): membrane potential at t;
C: whole-cell capacitance;
Gr = C*Gm/Cm, resting conductance;
Er, resting membrane potential (-55 mV);
Gm=$2e^{-5}$ S/cm^2; Cm=$1e^{-6}$ F/cm^2

The parameters, such as C and Er, are based on our experimental data. Gr was calculated by the following equation, where Gm is the specific membrane conducantce, Cm is the specific membrane capacitance (Hines, 1993).

Supplemental References

Hines, M. (1993). NEURON–a program for simulation of nerve equations. In Neural Systems: Analysis and Modeling, F.H. Eeckman, ed. (Norwell, MA: Kluwer Academic Publishers), pp. 127–136.

Liu, B.H., Wu, G.K., Arbuckle, R., Tao, H.W., and Zhang, L.I. (2007). Defining cortical frequency tuning with recurrent excitatory circuitry. Nat. Neurosci. 10, 1594–1600.

Wehr, M., and Zador, A.M. (2003). Balanced inhibition underlies tuning and sharpens spike timing in auditory cortex. Nature 426, 442-446.

Zhang, L.I., Tan, A.Y., Schreiner, C.E., and Merzenich, M.M. (2003). Topography and synaptic shaping of direction selectivity in primary auditory cortex. Nature 424, 201–205.

Zhou, Y., Liu, B.H., Wu, G.K., Kim, Y.J., Xiao, Z., Tao, H.W., and Zhang, L.I. (2010). Preceding inhibition silences layer 6 neurons in auditory cortex. Neuron 65, 706-717